Mesoporous Solid Acid

DOI: 10.1002/ange.200904791

Highly Active Mesoporous Nb–W Oxide Solid-Acid Catalyst**

*Caio Tagusagawa, Atsushi Takagaki, Ai Iguchi, Kazuhiro Takanabe, Junko N. Kondo, Kohki Ebitani, Shigenobu Hayashi, Takashi Tatsumi, and Kazunari Domen**

The synthesis of mesoporous transition-metal oxides has been extensively studied because of their wide range of potential applications.[1] Examples of such compounds include mesoporous TiO_2,[2,3] ZrO_2,[2,4] Nb_2O_5,[2,3b,5] Ta_2O_5,[2,6] $(Nb,Ta)_2O_5$,[2,7] SnO_2,[2,8] and WO_3,[2] which are used as a variety of heterogeneous catalysts, such as solid-acid catalysts,[4b,e,f,h,5d,6f,g] photocatalysts,[3b,f–h,6b,h] oxidation catalysts,[5c] and catalyst supports.[4d,g] Solid-acid catalysts, which are reusable and readily separable from reaction products, have been widely investigated as direct replacements for liquid acids to reduce the impact on the environment and to decrease costs. The use of mesoporous transition-metal oxides is an interesting approach to developing a solid-acid catalyst with enhanced activity. The mesopores in the oxide allows the reactants access additional active acid sites in the pores, resulting in improved rates of acid catalysis. Sulfated mesoporous niobium and tantalum oxides have been reported to exhibit remarkable activity in acid-catalyzed Friedel–Crafts alkylation and isomerization.[5d,6f,g] However, the use of the recycled catalyst remains difficult, a result of the leaching of sulfate species, as reported for mesoporous silica and organosilicas bearing sulfonic acid groups. Herein, mesoporous Nb–W mixed oxides are examined as solid-acid catalysts, these give very high catalytic performance in Friedel–Crafts alkylation, hydrolysis, and esterification, which originates from the mesoporous structure and different acid properties formed by specific Nb and W concentrations.

Mesoporous Nb–W mixed oxides were prepared from $NbCl_5$ and WCl_6 in the presence of a poly block copolymer surfactant Pluronic P-123 as a structure-directing agent. (Additional details are provided in the Supporting Information) Peaks attributable to mesopores were observed from $Nb_xW_{(10-x)}$ oxides with x values from 2 to 10 in the small-angle powder X-ray diffraction (XRD) pattern (see Figure S1 in the Supporting Information). Peaks attributed to (110) and (200) of the two-dimensional hexagonal structure were observed from an $x = 10$ sample (mesoporous Nb oxide), which was consistent with previous studies.[5] Wide-angle powder XRD patterns revealed the presence of crystallized tungsten oxide (WO_3) in W-rich samples ($x = 0$ to 2). The presence of mesopores was also indicated by the N_2 sorption isotherms (Figure 1) for the same samples ($x = 2$ to 10). The surface areas were estimated using the Brunauer–Emmett–Teller (BET) method, and pore volumes were obtained by the Barrett–Joyner–Halenda (BJH) method. Although the surface area decreased gradually from 200 (mesoporous Nb oxide) to 52 $m^2 g^{-1}$ (non-mesoporous W oxide) with increasing addition of W, up to $x = 0$, the pore volume decreased up to $x = 3$. Then, the pore volumes increased in the non-mesoporous W-rich oxides ($x = 0$ to 2) due to the formation of void spaces between particles (Supporting Information, Figure S2). The pore diameter obtained by the BJH method decreased from 7 (mesoporous Nb oxide) to 4.2 nm (mesoporous Nb_3W_7 oxide) with increasing W content, and mesopores were not observed in the Nb_1W_9 oxide (Supporting Information, Figure S3). SEM and TEM images of the porous

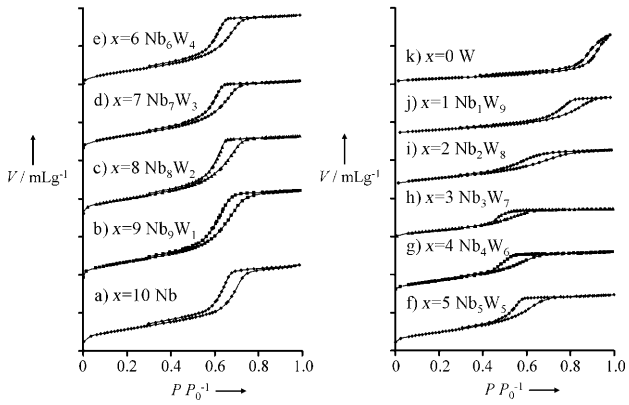

Figure 1. N_2 sorption isotherms of a) Nb, b) Nb_9W_1, c) Nb_8W_2, d) Nb_7W_3, e) Nb_6W_4, f) Nb_5W_5, g) Nb_4W_6, h) Nb_3W_7, i) Nb_2W_8 oxides and non-mesoporous j) Nb_1W_9 and k) W oxides. Traces are vertically shifted for clarity.

[*] C. Tagusagawa, Dr. K. Takanabe, Prof. K. Domen
Department of Chemical System Engineering, School of Engineering, The University of Tokyo
7-3-1 Hongo, Bunkyo-ku, Tokyo 113-8656 (Japan)
Fax: (+81) 3-5841-8838
E-mail: domen@chemsys.t.u-tokyo.ac.jp
Homepage: http://www.domen.t.u-tokyo.ac.jp

Dr. A. Takagaki, Prof. K. Ebitani
School of Materials Science, Japan Advanced Institute of Science and Technology (JAIST)
1-1 Asahidai, Nomi, Ishikawa 923-1292 (Japan)

A. Iguchi, Prof. J. N. Kondo, Prof. T. Tatsumi
Chemical Resources Laboratory, Tokyo Institute of Technology
4259 Nagatsuta Midori-ku, Yokohama 226-8503 (Japan)

Dr. S. Hayashi
Research Institute of Instrumentation Frontier, National Institute of Advanced Industrial Science and Technology (AIST)
Central 5, 1-1-1 Higashi, Tsukuba, Ibaraki 305-8565 (Japan)

[**] This work was supported by the Development in a New Interdisciplinary Field Based on Nanotechnology and Materials Science program of the Ministry of Education, Culture, Sports, Science and Technology (MEXT) of Japan and the Global Center of Excellence Program for Chemistry.

Supporting information for this article is available on the WWW under http://dx.doi.org/10.1002/anie.200904791.

oxides are shown in Figure 2. The mesoporous Nb oxide had hexagonally structured mesopores, as observed in the XRD pattern. The mesoporous Nb_7W_3, Nb_5W_5, and Nb_3W_7 oxides

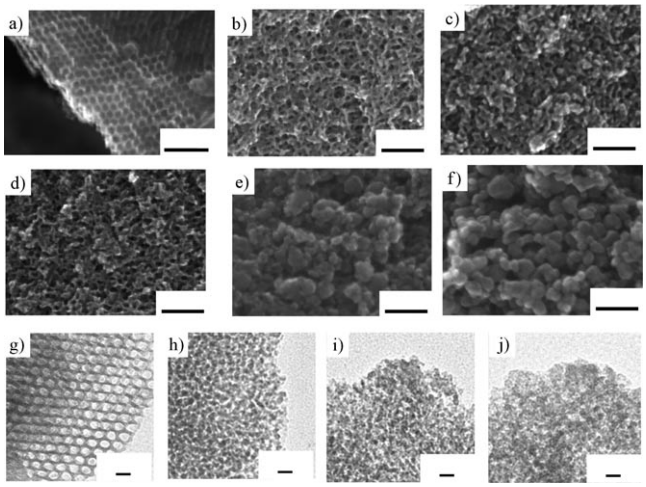

Figure 2. SEM images of mesoporous a) Nb, b) Nb_7W_3, c) Nb_5W_5, and d) Nb_3W_7 oxides (scale bar: 50 nm). SEM images of non-mesoporous e) Nb_1W_9 and f) W oxides (scale bar: 50 nm). TEM images of mesoporous g) Nb, h) Nb_7W_3, i) Nb_5W_5, and j) Nb_3W_7 oxides (scale bar: 10 nm).

had wormhole-type mesopores, and no mesoporous structure was observed in Nb_1W_9 or W oxides. Energy dispersive X-ray (EDX) spectroscopy analysis of Nb and W were carried out to correlate the initial stoichiometry and the resulting composition of the products (Supporting Information, Table S1). The average elemental compositions were very close to the initial stoichiometry, within 1% of differences for almost all the samples. However, considerable standard deviation could be observed for non-mesoporous W rich Nb_2W_8 (4%) and Nb_1W_9 (5%) oxides. The lack of uniformity was observed for samples with excess of W led to the formation of non-uniform structure by the calcination of the material at 673 K to remove the template, which induced the aggregation and crystallization of pure WO_3. The aggregation and crystallization resulted in the destruction of the original mesoporous structure and the development of larger pores (between 5.4 and 21.5 nm) for W rich $Nb_xW_{(10-x)}$ oxides (x = 0 to 2) as interparticle voids. The addition of the transition metal Nb to the W oxide should have improved the thermal stability of the material in the amorphous phase by elevating the crystallization temperature beyond that required to completely remove the mesoporous template (673 K). The same process could be observed for mesoporous TiO_2 oxides.[3i]

The acid-catalyzed reactions were first tested on the mesoporous $Nb_xW_{(10-x)}$ oxides using liquid-phase Friedel–Crafts alkylation of anisole with benzyl alcohol, and the hydrolysis of sucrose (a disaccharide composed of glucose and fructose) in water. A plot of the product yield of mesoporous $Nb_xW_{(10-x)}$ oxides with different Nb and W content in these reactions is shown in Figure 3. Variation of Nb and W content resulted in remarkably different reaction rates of benzylanisole formation in the alkylation. The reaction rates increased

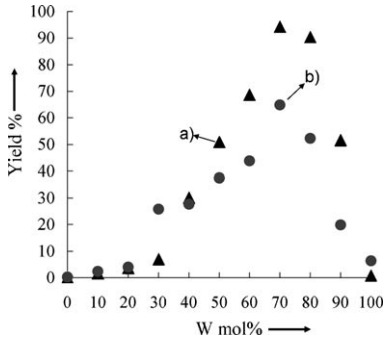

Figure 3. a) Friedel–Crafts alkylation of anisole (▲) and b) hydrolysis of sucrose (●) with mesoporous $Nb_xW_{(10-x)}$ oxides. Reaction conditions: (a) anisole (100 mmol), benzyl alcohol (10 mmol), catalyst (0.2 g), 373 K, 1 h, and (b) sucrose (0.5 g, 1.46 mmol), H_2O (10 mL, 556 mmol), catalyst (0.1 g), 353 K, 1 h.

gradually with increasing W content, starting from a 0% yield for mesoporous Nb oxide and reaching the highest yield (94%) for mesoporous Nb_3W_7 oxide. The yield decreased drastically for non-mesoporous oxide samples with x from 2 to 0, reaching 0% for W oxide. The same pattern was found for the hydrolysis of sucrose. The highest yield (65%) was obtained for mesoporous Nb_3W_7 oxide. These results indicate the importance of the mesoporous structure to the reaction, and demonstrate the drastic changes in the nature of the acid sites.

The acid properties of mesoporous $Nb_xW_{(10-x)}$ oxides were evaluated by probing the vibrational frequencies of adsorbed pyridine using Fourier transform infrared (FT-IR) spectroscopy. FT-IR spectra for pyridine adsorbed by mesoporous $Nb_xW_{(10-x)}$ oxides are shown in Figure 4. The tungsten-containing samples have both of Brønsted acid sites and Lewis acid sites whereas Nb oxide sample has negligible Brønsted acid sites. The FT-IR spectra indicate that the peak intensity at 1532 cm^{-1}, attributed to pyridinium ions formed on strong Brønsted acid sites,[9,10] was enhanced by increasing the W content. The Brønsted acid sites peak intensities have doubled from mesoporous Nb_7W_3 (2.5%) to Nb_5W_5 (5.0%)

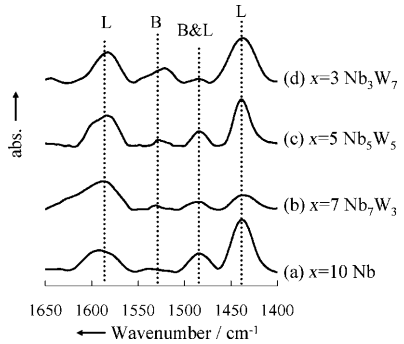

Figure 4. FT-IR spectra for pyridine adsorbed by mesoporous a) Nb, b) Nb_7W_3, c) Nb_5W_5, and d) Nb_3W_7 oxides. (B = Brønsted acid site; L = Lewis acid site) Assignments: 1590 cm^{-1} (strong Lewis acid site), 1532 cm^{-1} (strong Brønsted acid site), 1485 cm^{-1} (very strong Brønsted acid site or strong Lewis acid site), 1440 cm^{-1} (very strong Lewis acid site).

oxide and more than doubled from mesoporous Nb_5W_5 (5.0%) to Nb_3W_7 oxide (13.0%). The trend of Brønsted acid sites corresponded to the Friedel–Crafts alkylation rate, that is, the reaction was promoted by the Brønsted acid.[11]

The acid properties of mesoporous $Nb_xW_{(10-x)}$ oxides were also evaluated by ^{31}P magic-angle spinning (MAS) NMR spectroscopy, using trimethylphosphine oxide (TMPO) as a probe molecule. As the ^{31}P chemical shifts of protonated TMPO (that is, $TMPOH^+$) tended to move downfield, higher chemical shift values indicate higher protonic acid strength. The ^{31}P NMR spectra of mesoporous $Nb_xW_{(10-x)}$ oxides are shown in Figure 5. A total of 0.8 mmol of TMPO was

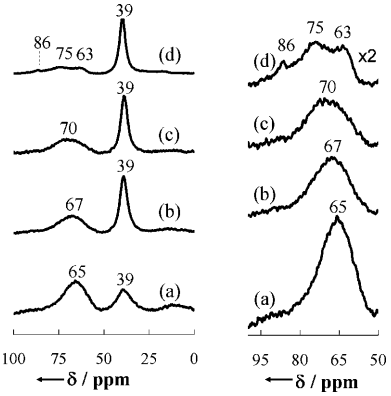

Figure 5. Left: ^{31}P MAS NMR spectra for TMPO adsorbed by mesoporous a) Nb, b) Nb_7W_3, c) Nb_5W_5, and d) Nb_3W_7 oxides, measured at room temperature. Right: enlargement of the acid-strength region. TMPO/catalyst: 0.8 mmol g^{-1}; the spinning rate of the sample was 10 kHz.

adsorbed per gram of mesoporous $Nb_xW_{(10-x)}$ oxide. Mesoporous Nb, Nb_7W_3, and Nb_5W_5 oxides had two principal peaks: a broad peak at $\delta = 65$–70 ppm and a sharp peak at $\delta =$ 39 ppm. The latter is ascribed to physisorbed TMPO.[12] Mesoporous Nb_3W_7 had three peaks indicating acid strength: a main peak at $\delta = 75$ ppm indicating acid strength comparable to that of H-Beta zeolite ($\delta = 78$ ppm),[13] another peak at $\delta = 63$ ppm indicating comparable strength to HY zeolite, ($\delta = 65$ ppm),[12] and a distinct small sharp peak at $\delta = 86$ ppm indicating acid strength greater that than that of ion-exchange resin ($\delta = 81$ ppm for Amberlyst-15) and comparable in strength to those of strongly acidic zeolites ($\delta = 86$ ppm for HZSM-5[14] and HMOR[13]) and sulfated zirconia.[15] The ^{31}P MAS NMR results show an enhancement of acid strength in mesoporous $Nb_xW_{(10-x)}$ oxides, with shifts of the main peaks from $\delta = 67$ ppm ($x = 7$) to $\delta = 70$ ppm ($x = 5$) or $\delta = 75$ ppm ($x = 3$). The acid strength of HY zeolite ($\delta = 65$ ppm) was be evaluated to $H_0 = -6.6$.[6g] Based on theoretical calculations, Zheng et al. proposed that a ^{31}P chemical shift of adsorbed TMPO above $\delta = 86$ ppm can be attributed to superacidity of the solid acid ($H_0 < -12$).[16] Therefore, it could be considered that mesoporous $Nb_xW_{(10-x)}$ oxides have a range of acid strength between $-12 \le H_0 < -6.6$. The total acid amounts were also estimated from the NMR peaks assigned to adsorbed TMPO. The acid amounts obtained were 0.30 mmol g^{-1} for Nb_3W_7, 0.36 mmol g^{-1} for Nb_5W_5, and 0.39 mmol g^{-1} for Nb_7W_3. The increase in acid amount corresponded to the increase in surface area, indicating that the acid density of mesoporous $Nb_xW_{(10-x)}$ oxides was constant.

The NH_3 temperature-programmed desorption (TPD) results for all the mesoporous $Nb_xW_{(10-x)}$ oxides were similar, with a main broad peak at 420–480 K and a shoulder peak above 515 K (Supporting Information, Figure S4). The shoulder peak positions were 570 K for mesoporous Nb_3W_7, 555 K for Nb_5W_5, 535 K for Nb_7W_3, reaffirming the acid strength order obtained from ^{31}P MAS NMR spectroscopy. Heats of adsorption for ammonia on Nb_3W_7, Nb_5W_5, Nb_7W_3, and Nb were estimated to be ca. 145, 140, 135, and 130 kJ mol^{-1}, respectively.

The acid catalytic activity of mesoporous Nb–W oxides was compared to that of conventional solid acids. The rate of glucose production and turnover frequency (TOF) for hydrolysis of sucrose over several solid-acid catalysts are shown in Figure 6. The hydrolysis of saccharides requires

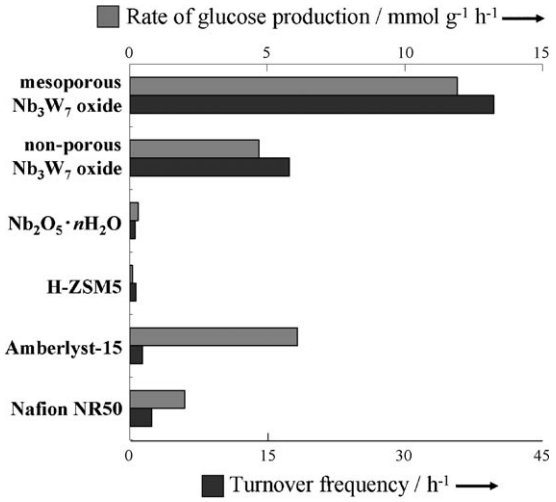

Figure 6. Hydrolysis of sucrose over several solid-acid catalysts. Reaction conditions: sucrose (0.5 g, 1.46 mmol), H_2O (10 mL, 556 mmol), catalyst (0.1 g), 353 K 1 h.

sufficient acid strength, and is an important class of reaction, used to convert biomass into bioethanol and other useful chemicals with minimal environmental impact.[17,18] Ion-exchange resins, such as Amberlyst-15,[18e] have strong sulfonic acid sites and as a result are powerful catalysts for the hydrolysis of saccharides. Niobic acid ($Nb_2O_5 \cdot n H_2O$) is a unique solid acid resistant in water solution.[19,20] The activity of mesoporous Nb_3W_7 oxide, however, substantially exceeded the maximum performance of any of the other materials tested, achieving a glucose production rate of 11.9 mmol $g^{-1} h^{-1}$. This reaction rate was significantly higher than that of niobic acid or H-ZSM5, and six times that of Nafion NR50 and two times that of Amberlyst-15. Moreover, the turnover frequency of mesoporous Nb_3W_7 was over 15 times that of Nafion NR50 and Amberlyst-15. The mesoporous Nb_3W_7 was recoverable by filtration and washing with water to remove residue, and the material was confirmed to

be reusable with no change in activity after three reuse cycles. The catalyst used in the first and third runs had glucose yields at 2 h of 85.9 and 84.1 %, respectively. The mesoporous Nb_3W_7 oxide also exhibited a reaction rate and turnover frequency twice that of bulk Nb_3W_7 oxide, indicating that the mesoporous structure enhanced the reaction rate of the accessible acid sites. Mesoporous $Nb_xW_{(10-x)}$ oxides were also tested for hydrolysis of cellobiose (Supporting Information, Table S2). The subunit of cellulose consists of β-1,4-glycosidic bonds, which are much more stable than the α-1,2-glycosidic bonds of sucrose, and are thus more resistant to hydrolysis.[18] Accordingly, the rate of glucose production by hydrolysis of cellobiose was much lower than that of sucrose over all of the acid catalysts tested. Nevertheless, mesoporous Nb_3W_7 oxide exhibited the highest rate of glucose production of the solid acids tested, including ion-exchange resins, niobic acid, and zeolites, and had a turnover frequency four-times that of sulfuric acid.

The acid amount and surface area of the tested solid acids, and the results of the Friedel–Crafts alkylation of anisole are summarized in Table S3 of the Supporting Information. Nonporous Nb_2O_5–WO_3[10] and $HNbWO_6$ nanosheet aggregates, obtained by exfoliation of layered $HNbWO_6$,[21] were also used for comparison. The mesoporous Nb_3W_7 oxide also exhibited the highest performance in this Friedel–Crafts alkylation reaction, giving the highest yield and turnover frequency. After the reaction, *ortho*-benzylanisole, *para*-benzylanisole, and dibenzylether were formed. The selectivity of *ortho*-benzylanisole over *para*-benzylanisole observed for mesoporous $Nb_xW_{(10-x)}$ oxides (Supporting Information, Table S3) on Friedel–Crafts alkylation gradually increased with increasing the W content (36.3 %, 40.3 %, and 42.4 % for mesoporous Nb_7W_3, Nb_5W_5, and Nb_3W_7 oxides, respectively). The same selectivity behavior towards *o*-benzylanisole could be observed for nonporous $Nb_xW_{(10-x)}$ oxides (Nb_7W_3, Nb_5W_5, and Nb_3W_7 oxides). The variation in selectivity should be caused not by mesoporous structures but by the variation of the acid properties (Brønsted acid and Lewis acid sites) of Nb and W concentrations. The selectivity of dibenzylether, a by-product of benzyl alcohol, was 18 %, 13 %, and 11 % for mesoporous Nb_7W_3, Nb_5W_5, and Nb_3W_7 oxides, respectively. These results are consistent with the results obtained by FT-IR spectroscopy, which show an increase in Brønsted acid sites (1532 cm^{-1}) correlates with a decrease in dibenzyl ether selectivity. However, dibenzyl ether is also a good alkylating agent and its concentration decreases as it is consumed together with the benzyl alcohol at the end of the alkylation reaction. The XRD analysis (Supporting Information, Figure S5) and SEM investigations (Supporting Information, Figure S6) indicate conservation of the mesoporous structures after the Friedel–Crafts alkylation. The mesoporous Nb_3W_7 oxide also showed high performance in the esterification of acetic acid and lactic acid with ethanol, exceeding the turnover frequencies of ion-exchange resins and zeolites (Supporting Information, Table S4).

In summary, worm-hole type mesoporous $Nb_xW_{(10-x)}$ oxides were found to function as recyclable, highly active mixed metal oxide solid-acid catalysts for Friedel–Crafts alkylation, hydrolysis, and esterification. The reaction rate and acid strength increased gradually with the addition of W, reaching the highest reaction rate with mesoporous Nb_3W_7 oxide, which exceeded the reaction rate of ion-exchange resins, zeolites, and non-mesoporous metal oxides. The very high catalytic performance of mesoporous Nb_3W_7 oxide was attributed to a high surface area mesoporous structure, strong acid sites which are comparable in strength to those of strongly acidic zeolites (HZSM-5 and HMOR), and the formation of strong Brønsted acid sites by the isomorphous replacement of Nb^{5+} ions by higher-valence W^{6+} ions in tungsten-enriched samples, as observed in WO_3/ZrO_2 ($H_0 = -14.6$).[22] In that case it is reported that replacement of ZrO_2 by WO_3 forms strong acid sites similar to that of SO_4/ZrO_2 ($H_0 = -16.1$).[22] The highest activity of WO_3/ZrO_2 was obtained at surface tungsten densities, which maximize the quantity of amorphous surface polytungstate species relative to the isolated surface WO_x and crystallized WO_3.[23] Similar to WO_3/ZrO_2, strong acid sites in the mesoporous Nb_3W_7 oxide could have formed leading to the high surface tungsten densities in the niobium matrix with no crystallized WO_3. Higher concentrations of W oxide deformed the mesoporous structure, decreasing the reaction rate. Mesoporous Nb_3W_7 oxide enabled both a high reaction rate and reusability, two essential characteristics of solid acids for industrial applications.

Received: August 27, 2009
Revised: October 18, 2009
Published online: December 28, 2009

Keywords: Friedel–Crafts alkylation · heterogeneous catalysis · mesoporous materials · metal oxides · solid acid

[1] a) A. Sayari, P. Liu, *Microporous Mater.* **1997**, *12*, 149 – 177; b) U. Ciesla, F. Schüth, *Microporous Mesoporous Mater.* **1999**, *27*, 131 – 149; c) F. Schüth, *Chem. Mater.* **2001**, *13*, 3184 – 3195; d) G. J. de A. A. Soler-Illia, C. Sanchez, B. Lebeau, J. Patarin, *Chem. Rev.* **2002**, *102*, 4093 – 4138; e) J. N. Kondo, K. Domen, *Chem. Mater.* **2008**, *20*, 835 – 847; f) Y. Rao, D. M. Antonelli, *J. Mater. Chem.* **2009**, *19*, 1937 – 1944.

[2] a) P. Yang, D. Zhao, D. I. Margolese, B. F. Chmelka, G. D. Stucky, *Nature* **1998**, *396*, 152 – 155; b) P. Yang, D. Zhao, D. I. Margolese, B. G. Chmelka, G. D. Stucky, *Chem. Mater.* **1999**, *11*, 2813 – 2826.

[3] a) D. M. Antonelli, J. Y. Ying, *Angew. Chem.* **1995**, *107*, 2202 – 2206; *Angew. Chem. Int. Ed. Engl.* **1995**, *34*, 2014 – 2017; b) V. F. Stone, Jr., R. J. Davis, *Chem. Mater.* **1998**, *10*, 1468 – 1474; c) Y. Yue, Z. Gao, *Chem. Commun.* **2000**, 1755 – 1756; d) H. Yoshitake, T. Sugihara, T. Tatsumi, *Chem. Mater.* **2002**, *14*, 1023 – 1029; e) H. Luo, C. Wang, Y. Yan, *Chem. Mater.* **2003**, *15*, 3841 – 3846; f) X. Wang, J. C. Yu, Y. Hou, X. Fu, *Adv. Mater.* **2005**, *17*, 99 – 102; g) Y. Shiraishi, N. Saito, T. Hirai, *J. Am. Chem. Soc.* **2005**, *127*, 12820 – 12822; h) G. Liu, Y. Zhao, C. Sun. F. Li, G. Q. Lu, H. M. Cheng, *Angew. Chem.* **2008**, *120*, 4592 – 4596; *Angew. Chem. Int. Ed.* **2008**, *47*, 4516 – 4520; i) J. N. Kondo, T. Yamashita, K. Nakajima, D. Lu, M. Hara, K. Domen, *J. Mater. Chem.* **2005**, *15*, 2035 – 2040.

[4] a) M. S. Wong, J. Y. Ying, *Chem. Mater.* **1998**, *10*, 2067 – 2077; b) Y. Y. Huang, T. J. McCarthy, W. M. H. Sachtler, *Appl. Catal. A* **1996**, *148*, 135 – 154; c) M. Mamak, N. Coombs, G. Ozin, *J. Am. Chem. Soc.* **2000**, *122*, 8932 – 8939; d) H. R. Chen, J. L. Shi, Y. S. Li, J. N. Yan, Z. L. Hua, H. G. Chen, D. S. Yan, *Adv. Mater.* **2003**,

15, 1078 – 1081; e) M. Chidambaram, D. Curulla-Ferre, A. P. Singh, B. G. Anderson, *J. Catal.* **2003**, *220*, 442 – 456; f) S. M. Landge, M. Chidambaram, A. P. Singh, *J. Mol. Catal. A* **2004**, *213*, 257 – 266; g) V. Idaliev, T. Tabakova, A. Naydenov, Z. Y. Yuan, B. L. Su, *Appl. Catal. B* **2006**, *63*, 178 – 186; h) C.-C. Hwang, C. Y. Mou, *J. Phys. Chem. C* **2009**, *113*, 5212 – 5221.

[5] a) D. M. Antonelli, J. Y. Ying, *Angew. Chem.* **1996**, *108*, 461 – 464; *Angew. Chem. Int. Ed. Engl.* **1996**, *35*, 426 – 430; b) B. Lee, D. Lu, J. N. Kondo, K. Domen, *J. Am. Chem. Soc.* **2002**, *124*, 11256 – 11257; c) T. Yamashita, D. Lu, J. N. Kondo, M. Hara, K. Domen, *Chem. Lett.* **2003**, *32*, 1034 – 1035; d) Y. Rao, M. Trudeau, D. Antonelli, *J. Am. Chem. Soc.* **2006**, *128*, 13996 – 13997.

[6] a) D. M. Antonelli, J. Y. Ying, *Chem. Mater.* **1996**, *8*, 874 – 881; b) Y. Takahara, J. N. Kondo, T. Takata, D. Lu, K. Domen, *Chem. Mater.* **2001**, *13*, 1194 – 1199; c) Y. Takahara, J. N. Kondo, D. Lu, K. Domen, *Chem. Mater.* **2001**, *13*, 1200 – 1206; d) K. Nakajima, M. Hara, K. Domen, J. N. Kondo, *Chem. Lett.* **2005**, *34*, 394 – 395; e) N. Shirokura, K. Nakajima, A. Nakabayashi, D. Lu, M. Hara, K. Domen, T. Tatsumi, J. N. Kondo, *Chem. Commun.* **2006**, 2188 – 2190; f) Y. Rao, J. Kang, D. Antonelli, *J. Am. Chem. Soc.* **2008**, *130*, 394 – 395; g) J. Kang, Y. Rao, M. Trudeau, D. Antonelli, *Angew. Chem.* **2008**, *120*, 4974 – 4977; *Angew. Chem. Int. Ed.* **2008**, *47*, 4896 – 4899; h) Y. Noda, B. Lee, K. Domen, J. N. Kondo, *Chem. Mater.* **2008**, *20*, 5361 – 5367.

[7] a) B. Lee, D. Lu, J. N. Kondo, K. Domen, *Chem. Commun.* **2001**, 2118 – 2119; b) T. Katou, D. Lu, J. N. Kondo, K. Domen, *J. Mater. Chem.* **2002**, *12*, 1480 – 1483; c) B. Lee, T. Yamashita, D. Lu, J. N. Kondo, K. Domen, *Chem. Mater.* **2002**, *14*, 867 – 875; d) T. Katou, B. Lee, D. Lu, J. N. Kondo, M. Hara, K. Domen, *Angew. Chem.* **2003**, *115*, 2484 – 2487; *Angew. Chem. Int. Ed.* **2003**, *42*, 2382 – 2385; e) D. Lu, T. Katou, M. Uchida, J. N. Kondo, K. Domen, *Chem. Mater.* **2005**, *17*, 632 – 637.

[8] a) K. G. Severin, T. M. Abdel-Fattah, T. J. Pinnavaia, *Chem. Commun.* **1998**, 1471 – 1472; b) F. Chen, M. Liu, *Chem. Commun.* **1999**, 1829 – 1830; c) T. Hyodo, N. Nishida, Y. Shimizu, M. Egashira, *Sens. Actuators B* **2002**, *83*, 209 – 215.

[9] a) E. P. Parry, *J. Catal.* **1963**, *2*, 371 – 379; b) T. R. Hughes, H. M. White, *J. Phys. Chem.* **1967**, *71*, 2192 – 2201.

[10] a) M. Hino, M. Kurashige, K. Arata, *Catal. Commun.* **2004**, *5*, 107 – 109; b) M. Hino, M. Kurashige, H. Matsuhashi, K. Arata, *Appl. Catal. A* **2006**, *310*, 190 – 193; c) K. Yamashita, M. Hirano, K. Okumura, M. Niwa, *Catal. Today* **2006**, *118*, 385 – 391.

[11] T. Shishido, T. Kitano, K. Teramura, T. Tanaka, *Catal. Lett.* **2009**, *129*, 383 – 386.

[12] E. F. Rakiewicz, A. W. Peters, R. F. Wormsbecher, K. J. Sutovich, K. T. Mueller, *J. Phys. Chem. B* **1998**, *102*, 2890 – 2896.

[13] H. M. Kao, C. Y. Yu, M. C. Yeh, *Microporous Mesoporous Mater.* **2002**, *53*, 1 – 12.

[14] Q. Zhao, W. H. Chen, S. J. Huang, Y. C. Wu, H. K. Lee, S. B. Liu, *J. Phys. Chem. B* **2002**, *106*, 4462 – 4469.

[15] W. H. Chen, H. H. Ko, A. Sakthivel, S. J. Huang, S. H. Liu, A. Y. Lo, T. C. Tsai, S. B. Liu, *Catal. Today* **2006**, *116*, 111 – 120.

[16] A. Zheng, H. Zhang, X. Lu, S. B. Liu, F. Deng, *J. Phys. Chem. B* **2008**, *112*, 4496 – 4505.

[17] a) J. N. Chheda, G. W. Huber, J. A. Dumesic, *Angew. Chem.* **2007**, *119*, 7298 – 7318; *Angew. Chem. Int. Ed.* **2007**, *46*, 7164 – 7183; b) A. Corma, S. Iborra, A. Velty, *Chem. Rev.* **2007**, *107*, 2411 – 2502.

[18] a) M. Sasaki, Z. Fang, Y. Fukushima, T. Adshiri, K. Arai, *Ind. Eng. Chem. Res.* **2000**, *39*, 2883 – 2890; b) A. Takagaki, C. Tagusagawa, K. Domen, *Chem. Commun.* **2008**, 5363 – 5365; c) S. Suganuma, K. Nakajima, M. Kitano, D. Yamaguchi, H. Kato, S. Hayashi, M. Hara, *J. Am. Chem. Soc.* **2008**, *130*, 12787 – 12793; d) A. Onda, T. Ochi, K. Yanagisawa, *Green Chem.* **2008**, *10*, 1033 – 1037; e) R. Rinaldi, R. Palkovits, F. Schüth, *Angew. Chem.* **2008**, *120*, 8167 – 8170; *Angew. Chem. Int. Ed.* **2008**, *47*, 8047 – 8050.

[19] a) T. Iizuka, K. Ogasawara, K. Tanabe, *Bull. Chem. Soc. Jpn.* **1983**, *56*, 2927 – 2931; b) K. Tanabe, S. Okazaki, *Appl. Catal. A* **1995**, *133*, 191 – 218; I. Nowak, M. Ziolek, *Chem. Rev.* **1999**, *99*, 3603 – 3624.

[20] a) T. Hanaoka, K. Takeuchi, T. Matsuzaki, Y. Sugi, *Catal. Today* **1990**, *8*, 123 – 132; b) T. Hanaoka, K. Takeuchi, T. Matsuzaki, *Catal. Lett.* **1990**, *5*, 13 – 16.

[21] C. Tagusagawa, A. Takagaki, S. Hayashi, K. Domen, *J. Phys. Chem. C* **2009**, *113*, 7831 – 7837.

[22] K. Arata, *Catal. Today* **2003**, *81*, 17 – 30.

[23] E. I. Ross-Medgaarden, W. V. Knowles, T. Kim, M. S. Wong, W. Zhou, C. J. Kiely, I. E. Wachs, *J. Catal.* **2008**, *256*, 108 – 125.

